Volume 66, Issue 5, 2022
Journal of Scientific Research
of
The Banaras Hindu University

Cationic and Anionic Substitutions in the Antibacterial and Biocompatibility Properties of Sol-Gel Derived Hydroxyapatite Nanocomposites

H. Sirajunisha[1,2], A. Krishnaveni[3], D. Sellathamil Selvaraj[1]and T.Balakrishnan[2*]

[1]*PG and Research Department of Physics, Bishop Heber College (Affiliated to Bharathidasan university), Tiruchirappalli – 620 017, Tamil Nadu, India. siraj.ph@bhc.edu.in*

[2]*Crystal Growth Laboratory, PG and Research Department of Physics, ThanthaiPeriyar Government Arts and Science College (Affiliated to Bharathidasanuniversity), Tiruchirappalli – 620 023, Tamil Nadu, India.* balacrystalgrowth@gmail.com

[3]*PG and Research Department of Zoology, National College (Affiliated to Bharathidasan university), Tiruchirappalli – 620 001, Tamil Nadu, India.*

Abstract: This paper deals the synthesis and characterization of Pure Hydroxyapatite (Pure HAp) nanopowderan its nanocomposites. Hydroxyapatite - Zinc (HAp-Zn), Hydroxyapatite - Manganese (HAp-Mn) Hydroxyapatite - Titanium (HAp-Ti) and Hydroxyapatite - reduced Graphene oxide (HAp-rGO). The impact of Zn, Mn, Ti and rGO on the underlying, morphological, antimicrobial property and biocompatibility of hydroxyapatite nanopowders are contemplated. The structural characterization analysed through XRD. Pure HAp, HAp-Ti and HAp-rGO displayed hexagonal structure and fuse of Zn and Mn in the host lattice changed the construction into orthorhombic and rhombohedral. The normal crystallite size goes from 51 nm to 37 nm for different nanocomposites. The consolidation of cations (Zn^{2+} Mn^{2+} and Ti^{4+}) and anion (CO_3^{2-}) diminished the crystallite size. Blended nanocomposites has hexagonal construction though there is hexagonal to orthorhombic progress in HAp-Zn and hexagonal to rhombohedral change in HAp-Mn nanocomposites The presence of functional groups in the samples is investigated utilizing FTIR examination. Surface morphology and compound organizations are examined utilizing Scanning Electron Microscope (SEM) and Energy Dispersive X-beam investigation (EDX) individually. The in-vitro antibacterial exercises and biocompatibility of the combined hydroxyapatite and its nanocomposite are examined utilizing Kirby-Bauer antibacterial testing and MTT assay individually. The outcomes show that Titanium and reduced Graphene Oxide fused hydroxyaptite nanocomposites are more harmful against every bacterial strain and didn't show any harmfulness against living tissues.

Keywords: Hydroxyapatite, Cation, Anion, Antibacterial, Biocompatibility, Bone, Implantation.

DIO: 10.37398/JSR.2022.660514

I. INTRODUCTION

Bone has traditionally been thought of as a static underlying organ that supports bodily development and protects the internal organs [1]. Biomaterials are materials that are natural structures that are created with real or fake parts. Biomaterials are in increasing demand for the fabrication of embed materials such as spinal, hip joints, knee problems, and so on [2]. To achieve the best results in the realm of muscular health, a material chosen for embed application must pass a consumption safety test and have mechanical and tribological properties [3]. As with physicochemical normal apatite [4-6], hydroxyapatite [$(Ca_{10}(PO_4)_6(OH)_2$] is a superb bioceramic material for calcified tissue fixing and recovery. It's a hexagonally structured clay formed of calcium phosphate bunches that look and feel like bone tissue. It has been widely used as a bone substitute as well as a substitution in a few therapeutic treatments due to its close chemical similarity to the typical inorganic bone lattice portion[7]. Despite the material's impressive capabilities, it has a few drawbacks, including low elasticity, low break durability, and a frail wear obstruction. The organic and physiochemical properties of hydroxyapatite can be improved by substituting particles found in normal bone apatite (cations Mg^{2+}, Zn^{2+}, Na^{+}, Mn^{2+}& Sr^{2+} or anions CO_3^2& HPO_4^2), and scientists have overcome the fundamental disadvantages of hydroxyapatite by modifying its structure with graphene subsidiaries, carbon nanotubes, polymers, TiO_2, ZrO_2, or ZnO [8-10].

Because of its antibacterial properties, ZnO nanoparticles have recently been widely used as a covering material for bone implant materials, particularly against Staphylococcus aureus and Escherichia coli. During medical procedures, this plays a key role in the development of bone-joint illnesses [11-15]. Because of its excellent biocompatibility, widespread erosion resistance, incredible mix of high strength and low modulus, high weakness and wear resistance, and high malleability, Ti compounds have been widely used as quick-arising insert materials [15,16,17]. Dental embeds and parts for orthodontic medical procedure, joint new parts for knee, shoulder, hip, spine, elbow and wrist, bone obsession materials like nails, screws and nuts, pacemaker and counterfeit heart valves, careful instruments, and so on are all examples of Ti and its amalgams being used in the pharmaceutical industry [18-20]. Manganese is a metal that may be found in organic apatite, such as bone and teeth. It is a major micronutrient, with a daily intake of 1–15 mg recommended. As it works on its mechanical qualities, fusing manganese into the apatite structure has piqued researchers' curiosity. It is also necessary for normal occurrences and the digestion of bones and muscles [21-25]. Graphene has piqued the interest of analysts in the preceding decade due to its exceptional features. The enhanced and consistent production of graphene subordinates, such as graphene oxide (GO) and reduced graphene oxide (rGO), brings up a slew of new possibilities in a variety of disciplines [26]. Because of their bioactive and biocompatible qualities, graphene-based nanocomposites are being pursued for biomedical applications as

substrates for SC separation, frameworks in tissue design, and portions of implantable devices [27,29]. Because its GO has a high explicit region, characteristic wrinkles, and a hydrophilic nature, it also has a good contact with the environment [28,30].

In light of the aforementioned studies, the underlying, morphological, and natural properties of Hydroxyapatite nanopowder and its composites, to be specific, are discussed in this work. Hydroxyapatite – Zinc (HAp-Zn), Hydroxyapatite – Titanium (HAp-Ti), Hydroxyapatite – Manganese (HAp-Mn), and Hydroxyapatite – Reduced Graphene Oxide (HAp-rGO) were produced, with improved antibacterial properties and biocompatibility.

II. EXPERIMENTAL TECHNIQUES

A. Materials and Methods

In the current study, starting antecedents were calcium nitrate tetra hydrate ($Ca(NO_3)_24H_2O$), orthophosphoric acid (H_3PO_4) and alkali (NH_3), zinc oxide (ZnO), manganese oxide (MnO), titanium dioxide (TiO_2), and reduced graphene oxide (rGO). To begin, DI water was used to make 025 M phosphoric acid. The pH of the mixture was adjusted to 10 by adding ammonia and stirring with a pretty stirrer. 1 M calcium nitrate tetra hydrate was prepared and progressively added to the aforesaid phosphoric acid – ammonia mixture, while maintaining a Ca/P ratio of 167. The mixture was then well stirred for 1 hour before being stored at room temperature for 24 hours to mature. The pure hydroxyapatite (Pure HAp) nanopowder was obtained by drying the gel at 65°C for 22 hours in a microwave. Then, using blended watery arrangements, hydroxyapatite-zinc (HAp-Zn), hydroxyapatite-manganese (HAp-Mn), hydroxyapatite-titanium (HAp-Ti), and hydroxyapatite – reduced graphene oxide (HAp-rGO) nanocomposites were included in the proportions 1:1, 1:1, 1:1, and 1:0.1, respectively, and the resultant suspensions was warmed in the hot air oven for different temperature and time to acquire the resultant composites [31].

B. Characterization techniques

The pre-arranged nanopowders and nanocomposites were investigated using a PANalytical/X Pert powder X-beam diffractometer with Cu K radiation (= 0.15406 nm); functional group examination using Fourier infrared spectroscopy (Perkin Elmer/Spectrum Two); and morphological and synthetic examination using filtering electron microscopy (CARL ZEISS/EVO18) and Energy Dispersive X-beam Analysis (The antibacterial properties and biocompatibility of the samples were further evaluated using individual agar-well-diffusion and MTT tests.

C. Antimicrobial Studies

The Kirby- Bauer plate - dispersion method, also known as the agar-well diffusion technique, is a cycle used to measure the antimicrobial specialist's impact on bacteria in culture. The sample was degraded in water and continuously mixed until a homogeneous colloidal suspension was formed to validate the antibacterial effect of the example on microorganisms using a good dispersion approach. The stock arrangement (1mg/ml) was broken up in a correct amount of refined water to give fluid centralizations of 50g/ml, 100g/ml, and 200g/ml of test. To test poisonousness against Escherichia coli,

Staphylococcus aureus, Pseudomonas aeruginosa, and Klebsiella pneumonia, a sufficient amount of these bacterial strains were washed delicately on the Muller Hinton agar medium and equitized wells were created. Three distinct focus suspensions of 50, 100, and 200 g/ml of the example, as well as sure and negative controls, were pumped into the various wells. Refined water was used as a negative control, while Tetracycline (30g/ml) was used as a positive control for E.coli and S.aureus, followed by ceftriaxone (30g/ml) for K. pneumonia and P.aeruginosa. For the time being, the plates were kept at 28°C for brooding. The zones of inhibition were measured in millimetres after the hatching period.

D. Cytotoxicity Test

The biocompatibility of organized nanocomposites was tested using a cytotoxicity test. The National Center for Cell Science in Pune provided human cellular breakdown in the lungs cell line A549 for this study. Corning, in the United States, provided the plastics, reagents, and media.

E. Cell Viability Assay

50,000 cells were grown in 96-well plates and brooded for 24 hours under conventional culture conditions.The medium was removed after 24 hours. A new media containing unadulterated hydroxyapatite test in fixation ranging from 5M to 75M was given to the cells, and they were again hatched for another 24 hours. The medium with pure hydroxyapatite test was removed after the brooding period. 1X PBS was used to wash the cells. Following the washing, 100l of MTT dye (at a concentration of 5mg/ml) was applied to the cells. The cells were treated with MTT dye for 3 hours. The medium was gently removed after 3 hours without disturbing the Formosan stones. In 100 litres of fermented isopropanol, the Formazan diamonds framed by the movement of practical cells were broken down. At 570 nm, the purple shading arrangement was examined, using a reference frequency of 630 nm.

III. RESULT AND DISCUSSIONS

A. Structural Analysis:

Fig.1. shows the powder X-ray diffraction patterns of pure HApnanopowder and its composites. It reveals the various qualities of diffraction peaks associated with pure HAp as indicated by JCPDS card No: 74-0566, HAp-Zn as indicated by JCPDS card No: 71-0889, HAp-Mn as indicated by JCPDS card No: 70-0009, HAp-Ti as indicated by JCPDS card No: 84-1286, and HAp-rGO as indicated by JCPDS card No: 19- When compared to Zn, Ti, and Mn included samples, pure and rGO-HAp samples had more widespread peaks, indicating that they have lower crystallinity than HAp-Zn, HAp-Ti, and HAp-Mn nanocomposites [32,33,34]. In the HAp-Zn, HAp-Ti, and HAp-Mn composites, the intensity of the transcendence planes (020) increases, and the 2θ amounts show a little difference when compared to pure HApnanopowder[35,36,37].This is because of the incorporation of zinc, titanium and manganese into the structure of hydroxyapatite nanopowders.

The mean crystallite size and lattice strain may be calculated from the XRD peaks. Williamson and Hall (W-H) strategy, Warren Averbach (W-A) Analysis, Reitveld refinement, and Pseudo Voigt work are some of the methodologies for calculating these values [37,39]. The Debye Scherrer formula [38] is used to calculate the crystallite size (d) in this article.

For the unadulterated HAp, HAp-Zn, HAp-Mn, HAp-Ti, and HAP-rGO(1:0.5:0.1) samples, d = 0.9λ / βcosθ are 50.9 nm, 46.9 nm, 47.8 nm, 46.1 nm, 37.4 nm, respectively (where, λ = 1.5406 Å) Because the nuclear range of cations (Mn>Zn>Ti) is not as large as calcium's and carbon is not precisely phosphorous, the usual crystallite size shrinks with cationic and anionic replacements [40-43].

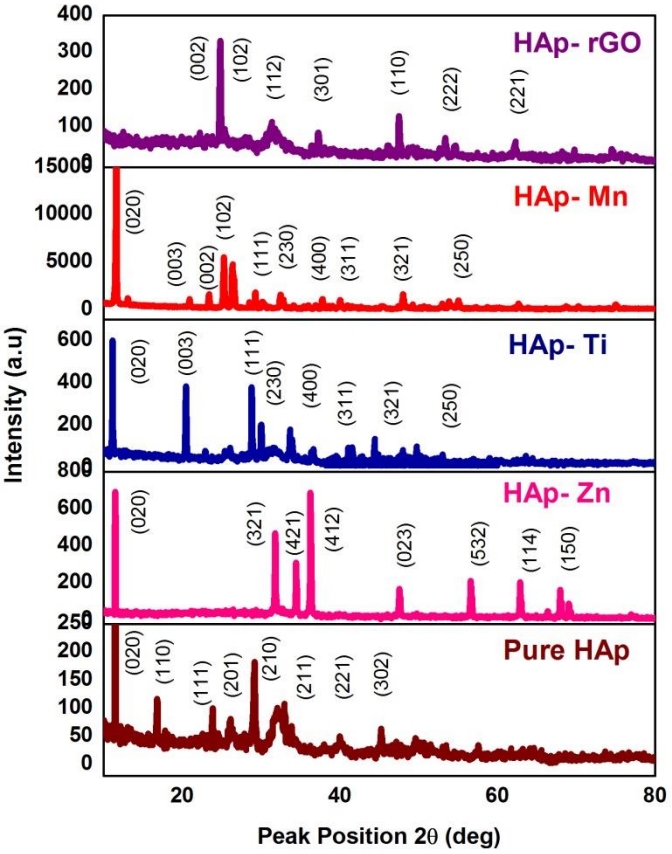

Fig. 1. Powder X-Ray Diffraction Pattern

The hexagonal structure of hydroxyapatite (space bunch P63/m) has 44 molecules per unit cell. The hydroxyapatite unit cell is depicted in Figure 2(a). In the hydroxyapatite structure, there are two distinct Ca destinations. The main calcium site, Ca (I), is surrounded by nine oxygen particles from the adjacent phosphate tetrahedron, whereas the secondary calcium site, Ca (II), is surrounded by six oxygen particles from phosphate and hydroxy groupings. Three oxygen particles are classified as O1, O2, and O3 based on their distance and coordination number with calcium. The oxygen in a hydroxyl bunch is denoted by the letter OH. As a result, the HAp recipe may be written as $Ca(I)_4$ $Ca(II)$ $_6(PO1O2(O3)_2)_6(OHH)_2$ [44]. Ca-O, P-O, and O-H are three different types of holdings in HAp. Ca-O is ionic, whereas P-O and O-H are covalent [45].

The substitution of cations and anions in the hydroxyapatite structure was used to account for the number of studies [46,47]. According to these findings, cations replace calcium particles, whereas anions replace phosphate or hydroxyl particles. Zn^{2+} and Mn^{2+} ions substitute Ca^{2+} ions at any of the Ca destinations in the HAp-Zn and HAp-Mn structures, as shown in Figs. 2(c) and 2(d). Because Ca^{2+}, Zn^{2+}, and Mn^{2+} have comparable valence states, there will be no charge pay defects in that ionic bond [48,49].

Zinc, on the other hand, has more susceptible ionic connections in hydroxyapatite than manganese and calcium due to the modification of their nuclear span [50]. In the HAp-Zn test, there is hexagonal to orthorhombic advancement, and in the HAp-Mn test, there is hexagonal to rhombohedral change, where combination temperature plays a key role [51, 52]. As shown in Fig. 2e [53], Ti^{4+}particle substitutes Ca^{2+}particle at any of the Ca destinations in the HAp-Ti complex. Because $Ca^{2+}$and Ti^{4+} have different valence states, two H^+ were simultaneously removed from the hydroxyl

gathering in order to get charge remuneration while Ca was replaced by Ti [54,55]. The grid limits of the HAp-Ti are shown in Table 1, confirming hexagonal architecture [56]. CO_3^{2-}particle substitutes OH^-(A type) orPO_4^{3-}(B type) particle in the hydroxyapatite structure in the HAp-rGO structure. Among them, the B type is the most common, with a decrease in the a-axis length and an increase in the c-axis length [57]. The carbonate particle clearly substitutes any phosphate particle in Fig. 2(f).

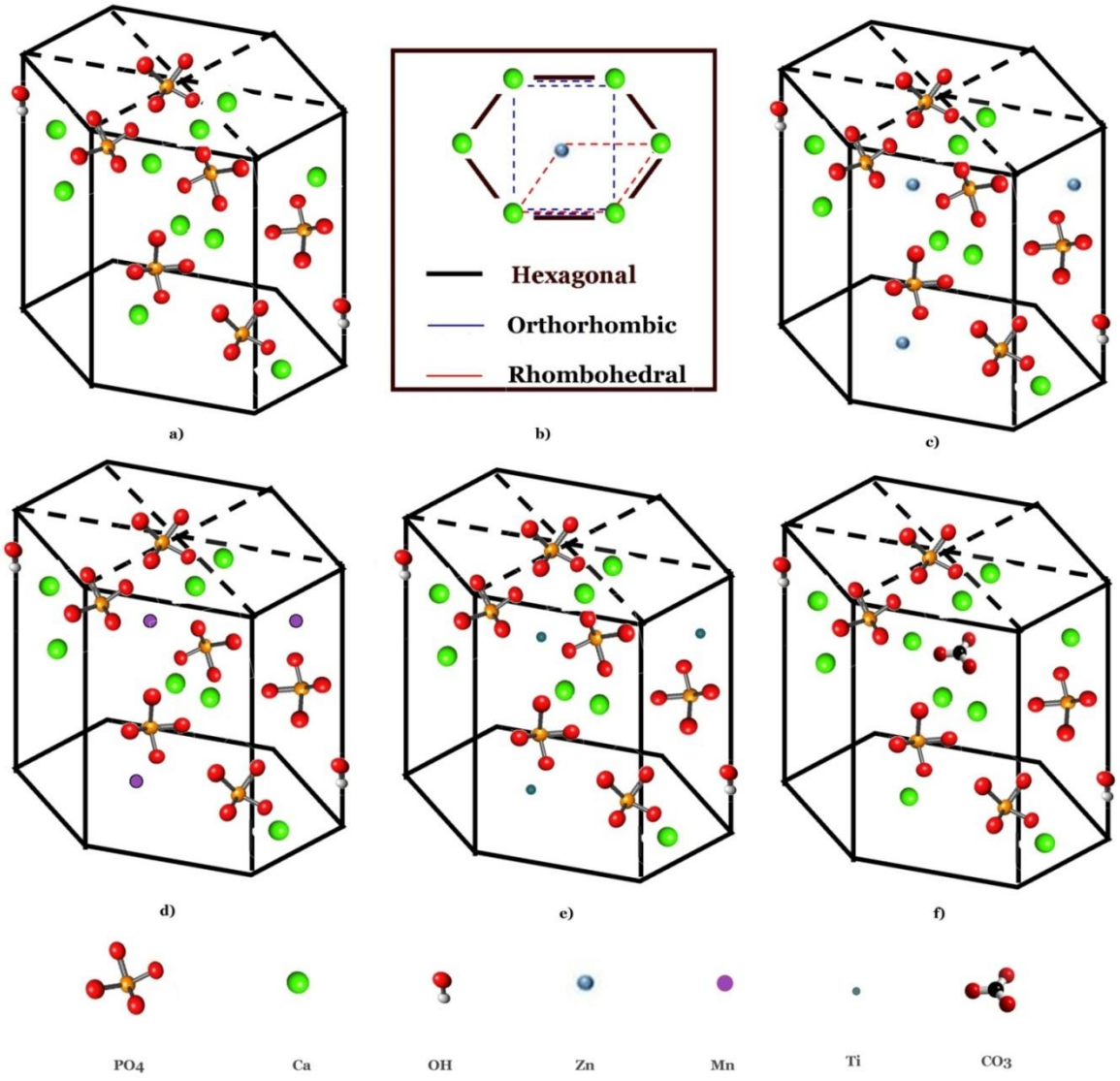

Fig. 2. Bonding mechanisms of doped and undoped-HAp a) Pure HAp b)General View of Transition c) Zn-HAp d)Mn-HAp e)Ti-HAp f)rGO-HAp

Table I: IR peaks and their assignments for the prepared samples

Observed Band Positions (cm^{-1})					Assignment
Pure HAp	**HAp-Zn**	**HAp-Mn**	**HAp-Ti**	**HAp-rGO**	
3397	3409	3487	3487	3418	O-H symmetric stretching
2402	2363	3409	2361	2426	H-P-O asymmetric stretching
-	-	-	-	1635	C=O asymmetric stretching
-	-	-	-	1435	C=O symmetric stretching
1386	1379	1403	1317	1385	H-P-O bending
1127	1036	1061	1063	1034	O-H bending
-	-	-	-	906	C-O stretching vibration
-	-	-	651	-	Ti-O symmetric stretching
-	562	-	-	-	Zn-O stretching vubration
-	-	791,874	-	-	Mn-O symmetric & asymmetric stretching

B. FTIR Spectral Analysis:

The FTIR range obtained in the range 400–4000 cm-1 was used to track the beneficial groups contained in pure HApnanopowder and its composites (Fig. 3). Table 1 shows the locations of the bands that were detected, as well as their individual peaks. The comparison band locations for H-P-O, P-O, and O-H groups are different, as shown in figure 4, and are in perfect agreement with the hallmark FTIR information for hydroxyapatite crystal phases [45].

In addition, the HAp-Zn composites [58] have the Zn–O (562 cm-1) band position, while the HAp-Mn (792, 873 cm-1) composites have the Mn–O band position. In the HAp-Ti composites [60,61], the Ti-O band position (651, 602, and 601 cm-1) is also accessible. Carbonate apatite (1635, 1640, 1642, 1436, 1400, 1401, 906, 962, and 963 cm-1) has been discovered in the HAp-rGO composite [62,63]. This signal attributed to the C=O and C-O groups suggests that graphene in that sample is linked.

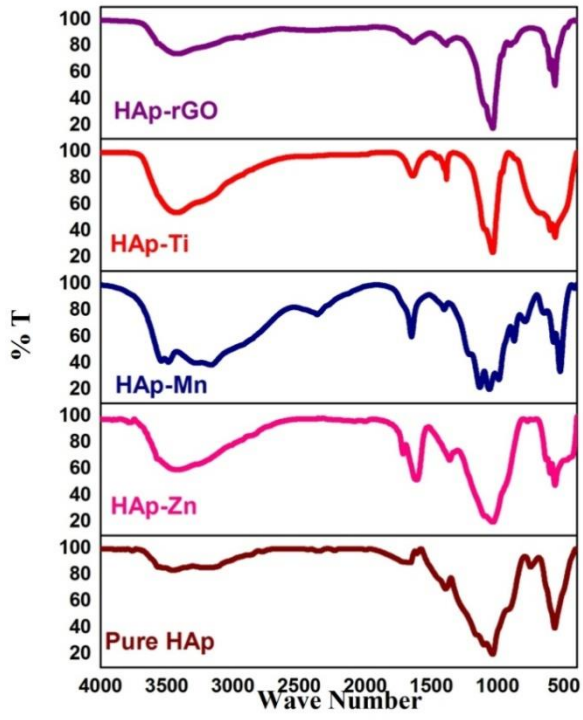

Fig. 3. Fourier Transform Infra-Red Spectra

C. SEM and EDAX Analysis

Using a scanning electron microscope, the morphology of the produced nanocomposites was studied (SEM). SEM micrographs and EDAX spectra of pure HApnanopowder and its composites at nanometer scale are shown in Figure 4.

The SEM micrographs clearly show that particles in pure HAp are randomly distributed. Nanorod structures are observed in HAp-Zn [58], ambiguous polycrystalline features are evident in HAp-Mn [64], and platelets and nanospheres are present in HAp-Ti [61]. Nanoflakes are framed on agglomerated spheres in HAp-rGO [63]. This is due to the individual consideration of Zn, Mn, Ti, and rGO in the hydroxyapatite nanopowder.

The electron magnifying device equipped with Energy Dispersive Analysis employing X-beams (EDAX) was used for precise compositional analysis. The range confirms the existence of Zn, Mn, Ti, and C in hydroxyapatite composites.

The pure hydroxyapatite test clearly contains calcium (Ca), phosphorus (P), and oxygen (O); the HAp-Zn sample contains calcium (Ca), phosphorus (P), oxygen (O), and zinc (Zn); the HAp-Mn sample contains calcium (Ca), phosphorus (P), oxygen (O), and manganese (Mn); the HAp-Ti sample contains calcium (Ca), phosphorus (P), oxygen (O) and titanium(Ti).

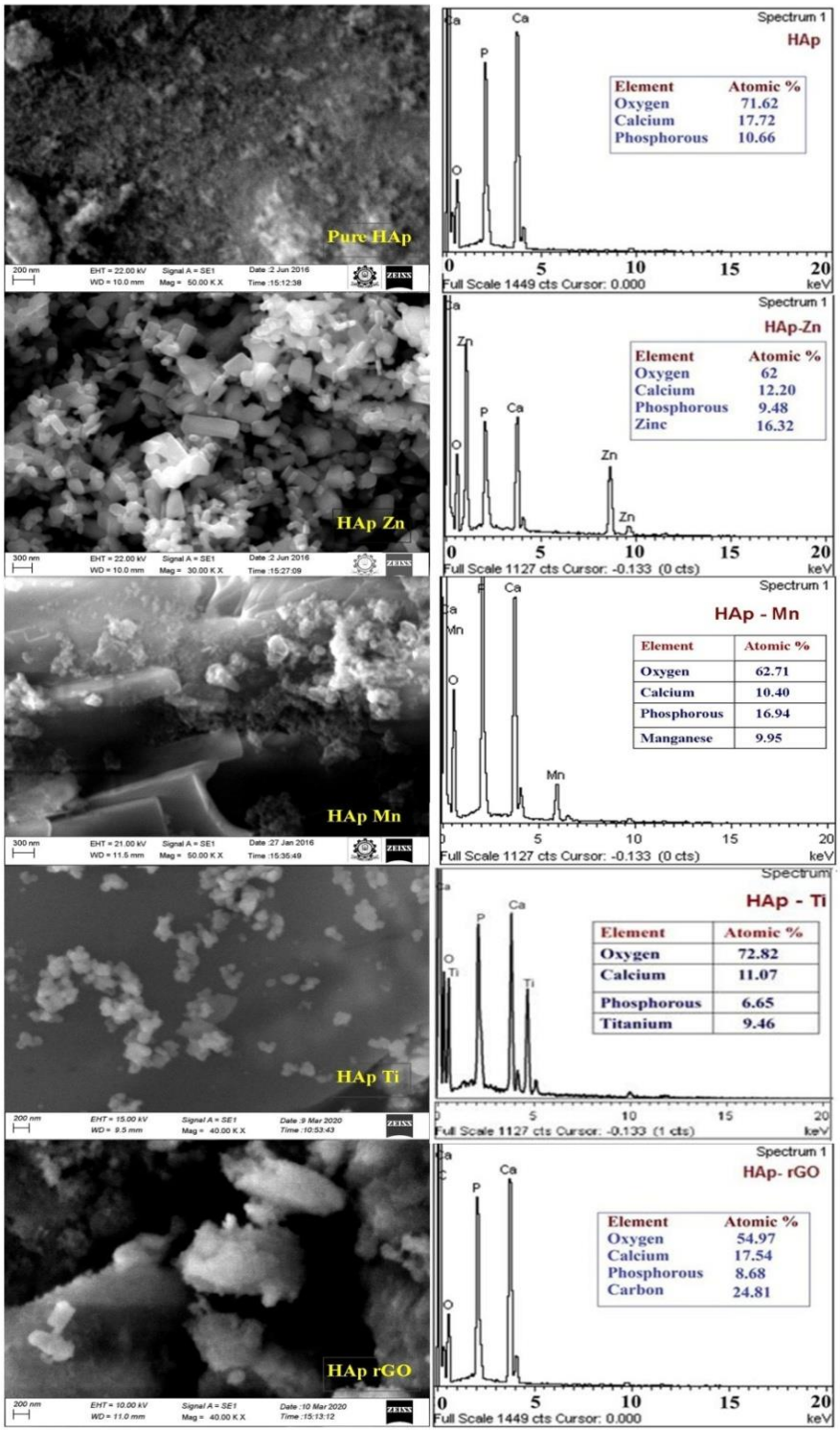

Fig. 4. SEM Micrographs and EDAX Spectra of Pure Hydroxyapatite and its Composites

D. Antibacterial Activity:

The antibacterial characteristics of mixed nanocomposites were tested using the Agar-well diffusion method in this study. E.coli, Pseudomonas aeruginosa, Staphylococcus aureus, Klebsiella pneumoniae, and Proteus vulgaris were the test organic entities used in the study.

Pseudomonas aeruginosa (64.3%) was the most common segregate generating post-employable injury contaminations, particularly in bone and joint illnesses, followed by Staphylococcus aureus (14.3%), Klebsiella pneumonia (10%), E.coli (5.7%), and Proteus species (5.7%) [65]. Four of the five microorganisms are chosen for the review because hydroxyapatite nanopowder and its composites are viable bone implant replacements.

The findings of antibacterial activity using the agar – well diffusion technique are shown in Figure 5. The antibacterial activity was assessed by the size of inhibitory zones (mm). The zinc and titanium combined hydodroxyaptite nanocomposites were clearly more effective against all four animals, as seen in the picture. This is due to the arrival of Zn^{2+} particles into the advancement media, and the impedance of Zn^{2+} particles with the protein systems of microorganisms by evacuating with magnesium particles, which is essential for bacterial enzymatic activities [66,67], as well as the arrival of Ti^{4+} particles into the advancement media, and Hydroxyapatite has a high partiality for proteins, and Ti subbed HAp create positive openings, similar to TiO_2impetuses.The structured positive apertures interact with adsorbed H_2O to produce hydroxyl extremists (OH^-), which have a substantial oxidation capability and may break down a variety of natural materials, demonstrating the bactericidal effect. In a similar vein, hydroxyapatite modified with Ti4+ particles displays antibacterial properties [67]. Zn-HAp and Ti-HAp are more effective against each of the four bacteria, but HAp-rGO is more effective at greater doses. [68,69]. This might treat post-workplace injury disorders and bone joint infections at an early stage without identifying the major driver of the relevant microbe, allowing for a number of advancements in current clinical medicine [66,70].

E. MTT Assay

The results of the MTT Assay demonstrating Biocompatibility of organised instances in human cellular breakdown in the lungs cell line A549. The results reveal that the integrated instances had no cytotoxicity when tested against the malignant development cell line A549, which has a high level of biocompatibility. The feasibility of the nanocomposites ranges between 87 to 97, with HAp-Ti nanocomposites having a degree of reasonability of 97. Furthermore, HAp-Mn and HAp-rGO nanocomposites perform similarly to HAp-Ti nanocomposites, with 96 and 95 levels of practicality, respectively. The biocompatibility of manganese, titanium, and reduced graphene oxide nanocomposites has improved in recent years. [71-75].

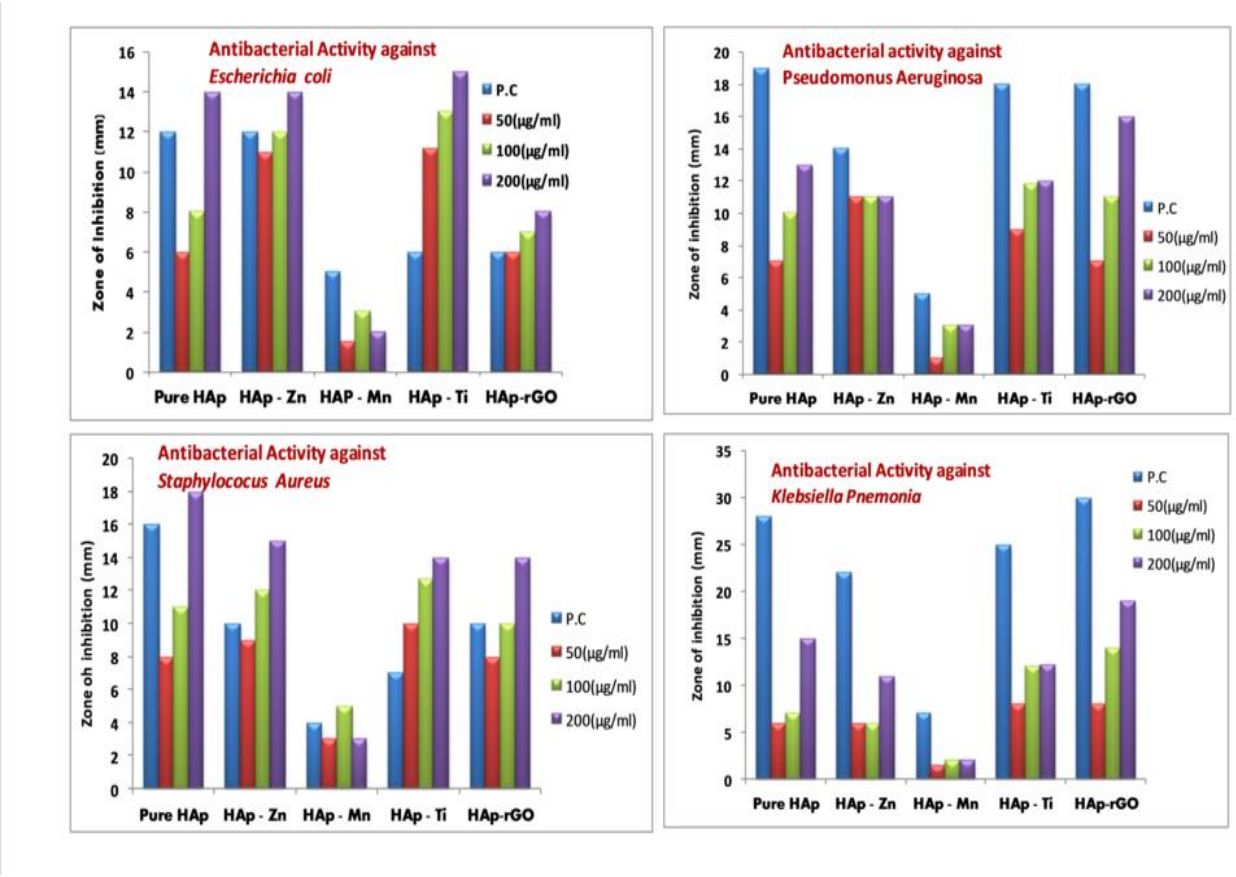

Fig. 5. Antibacterial activity of prepared samples against Pathogenic Bacterial Strains

Table II: Average crystalline size, zone of inhibition and percentage of viability of various samples

Sample	D (nm)	Maximum Zone of Inhibition (mm)				Max % of Viability
		E.Coli	*P.Aeruginosa*	*K.Pneumonia*	*S.Aureus*	
Pure HAp	50.9	14	13	15	**18**	87
HAp-Zn	46.9	14	11	11	15	88
HAp-Mn	47.8	5	5	4	6	96
HAp-Ti	46.1	**15**	12	12	14	**97**
HAp-rGO	37.4	8	**16**	**19**	14	95

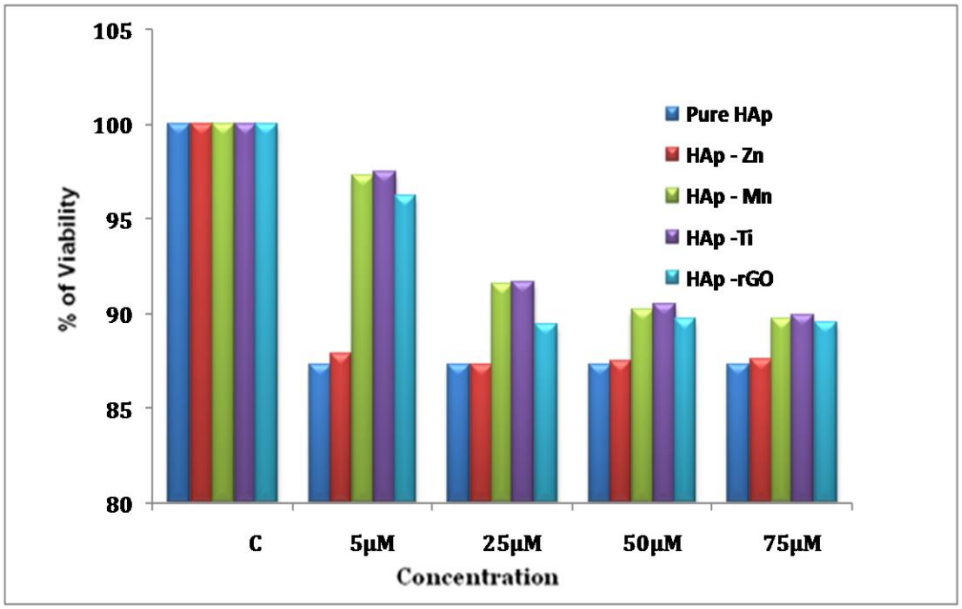

Fig. 6. Results of MTT Assay demonstrating Biocompatibility of prepared samples tested in human lung cancer cell line A549

IV. CONCLUSION

The sol-gel approach was used to successfully produce hydroxyapatite nanopowder and its composites (HAp-Zn, HAp-Mn, HAp-Ti, and HAp-rGO) using calcium nitrate tetra hydrate, phosphoric acid, ammonia, zinc oxide, manganese oxide, titanium dioxide, and graphene oxide as starting materials. For the integrated instances, XRD and FTIR investigations were used. The samples have hexagonal construction, with hexagonal to orthorhombic advance in HAp-Zn nanocomposites and hexagonal to rhombohedral change in HAp-Mn nanocomposites, and the typical crystallite size was 45 nm, according to XRD data. The presence of functional groups in the prepared samples is confirmed by the FTIR range. SEM analysis showed the formation of nano agglomerates in all of the samples. Pure HAp particles were randomly spread, HAp-Zn nanorod structures were there, HAp-Mn vague polycrystalline characteristics were formed, HAp-Ti platelets and nanospheres were present, and HAp-rGO particles were agglomerated. The presence of compound components in the produced samples is confirmed by EDAX analysis. The antibacterial experiments revealed that titanium substituted nanocomposites (HAp-Ti) 100 percent effective against diverse microbes, followed by

HAp-rGO and HAp-Zn samples. When tested by MTT in the human cellular breakdown in the lungs cell line, the cytotoxicity test reveals that all of the samples are biocompatible, and the HAp-Mn, HAp-Ti, and HAp-rGO tests demonstrate the highest degree of reasonability. As a result, ion substituted hydroxyapatite nanocomposites have improved antibacterial activity and biocompatibility, making them more hazardous to bacteria while being safe for human consumption. Novel HAp-rGO-M composites will be ready in the near future to further enhance their mechanical and organic characteristics in order to create intensive dental and implant materials.

REFERENCES

[1] A. Oryan, S. Alidadi, A. Moshiri, Current concerns regarding healing of bone defects,Journal of Hard Tissue Biology. 2 (2013) 1–13. https://doi.org/10.13172/2050-2303-2-2-374

[2] M. Geetha, A.K. Singh, R. Asokamani, A. K. Gogia, Ti based biomaterials, the ultimate choice for orthopaedic implants – A review, Progress in Materials Science. 54 (2009) 397–425. https://doi.org/10.1016/j.pmatsci.2008.06.004

[3] Y. Xie, H.L i, C. Zhang, X. Gu, X. Zheng, L. Huang, Graphene- reinforced calcium silicate coatings for load-bearing implants, Biomedical Materials. 9 (2014) 025009–025015. https://doi.org/10.1088/1748-6041/9/2/025009.

[4] E. Damien, P.A. Revell, Coralline hydroxyapatite bone substitute: A review of experimental studies and biomedical applications, Journal of Applied Biomaterials & Biomechanics, 2 (2004) 65–73. https://doi.org/10.1177/228080000400200201

[5] G. Wei, P. X. Ma, Structure and properties of nano-hydroxyapatite/polymer composite scaffolds for bone tissue engineering, Biomaterials. 25 (2004) 4749–4757. https://doi.org/10.1016/j.biomaterials.2003.12.005

[6] N. Kantharia, S. Naik, S. Apte, M. Kheur, S. Kheur, B. Kale, Nano hydroxyapatite and its Contemporary applications, Journal of Dental Research. 1 (2014) 15–19. https://doi.org/10.4103/2348-3407.126135

[7] D.W. Hutmacher, J.T. Schantz, C.X.F. Lam, K.C. Tan, T.C. Lim, State of the art and future directions of scaffold-based bone engineering from a biomaterials perspective, Journal of Tissue Engineering and Regenerative Medicine. 1 (2007) 245–260. https://doi.org/10.1002/term.24

[8] Feng Chen, Ying-jie Zhu, Jin Wu, Peng Huang, DaxiangCui, Nanostructured calcium phosphates: preparation and their application in biomedicine, Nano Biomedicine and Engineering. 4(2012) 41–49. https://doi.org/10.5101/nbe.v4i1.p41-49

[9] D. Sivaraj, K. Vijayalakshmi, Enhanced corrosion resistance and antibacterial activity of Zn-HA decorated MWCNT's film coated on medical grade 316L SS implant by novel Spray pyrolysis technique, Journal ofAnaitical and Applied Pyrolysis. 134 (2018) 176–182. https://doi.org/10.1016/j.japp.2018.06.006

[10] J. Seil, T. Webster, Reduced Staphylococcus aureus proliferation and biofilm formation on zinc oxide nanoparticle PVC composite surfaces, ActaBiomaterialia 7 (2011) 2579–2584. https://doi.org/10.1016/j.actbio.2011.03.018

[11] R. Kumar, P. Sakthivel, P. Mani, Structural, optical, electrochemical, and antibacterial features of ZnS nanoparticles: incorporation of Sn, Applied Physics A125 (2019) 543. https://doi.org/10.1007/s00339-019-2823-2

[12] M. Vargas-Reus, K. Memarzadeh, J. Huang, G. Ren, R. Allaker, Antimicrobial activity of Nanoparticulate metal oxides against peri-implantitis pathogens, InternationalJournal ofAntimicrobial Agents. 40 (2012) 135–139. https://doi.org/10.1016/j.ijantimicag.2012.04.012.

[13] R. Darouiche, Treatment of infections associated with surgical implants. The New EnglandJournal of Medicine. 350 (2004) 1422–1429.https://doi.org/10.1056/NEJMra035415

[14] R.Sarvan Ricky, M. KikaniKunjan, J. Assudani Hitesh, Mehta Sanjay, Bacteriological study of post operative wound infections and antibiotic susceptibility pattern of the isolates, Biennial Journal of GAPM. 6 (2017).http://dx.doi.org/10.18203/2349-3933.ijam20195166

[15] K. Kotlhao , M. D.T. Madiseng, F. M. Mtunzi1 , V. E. Pakade , S. J. Modise , N. Laloo, M. J. Klink, The synthesis of silver, zinc oxide and titanium dioxide nanoparticles and their antimicrobial activity, Advanced Materials. Pocedings. 2 (2017) 479–484. https://doi.org/10.5185/amp.2017/803

[16] Long M, Rack HJ, Titanium alloys in total joint replacement--a materials science perspective, Biomaterials. 19 (1998) 1621–1639.https://doi.org/10.1016/s0142-9612(97)00146-4

[17] Pilliar R.M. (2021) Metallic Biomaterials. In: Narayan R. (eds) Biomedical Materials. Springer, Cham. http://doi-org-443.webvpn.fjmu.edu.cn/10.1007/978-3-030-49206-9_1

[18] M. Vargas-Reus, K. Memarzadeh, J. Huang, G. Ren, R. Allaker, Antimicrobial activity of Nanoparticulate metal oxides against peri-implantitis pathogens, InternationalJournal ofAntimicrobial Agents.40 (2012) 135–139. https://doi.org/10.1016/j.ijantimicag.2012.04.012.

[19] R. Darouiche, Treatment of infections associated with surgical implants. New England Journal of Medicine. 350 (2004) 1422–1429.https://doi.org/10.1056/NEJMra035415

[20] K. Kotlhao , M. D.T. Madiseng, F. M. Mtunzi1 , V. E. Pakade , S. J. Modise , N. Laloo, M. J. Klink, The synthesis of silver, zinc oxide and titanium dioxide nanoparticles and their antimicrobial activity, Advanced Materials. Pocedings.2 (2017) 479–484. https://doi.org/10.5185/amp.2017/803

[21] A.N. Natasha , I. Sopyan , A. Zuraidac,Fourier Transform Infrared Study on Sol-Gel Derived Manganese-doped Hydroxyapatite,Advanced Materials Research. 47-50 (2008) pp 1185-1188http://dx.doi.org/10.4028/www.scientific.net/AMR.47-50.1185

[22] D. Yan, S. Cheng, R. F. Zhuo et al., "Nanoparticles and 3D sponge-like porous networks of manganese oxides and their microwave absorption properties," Nanotechnology, 20 (2009).https://iopscience.iop.org/article/10.1088/0957-4484/20/10/105706.

[23] T. Ahmad, K. V. Ramanujachary, S. E. Lofland, and A. K. Ganguli, "Nanorods of manganese oxalate: a single source precursor to different manganese oxide nanoparticles (MnO, Mn_2O_3, Mn_3O_4)," Journal ofMaterials Chemistry. 14 (2004) 3406–3410. https://doi.org/10.1039/B409010A

[24] Yang P, Klimis-Tavantzis D. Effects of dietary manganese on arterial glycosaminoglycan metabolism in Sprague–Dawley rats. Biological Trace Element Research. 64 (1998) 275–288.

[25] Kolmas J, Jablonski M, Ślósarczyk A, Kolodziejski W. Solid-state NMR study of Mn2+ for Ca2+ substitution in thermally processed hydroxyapatites. Journal of American Ceramic Society. 2014. doi:10.1111/jace.13394.

[26] L. Zhang, X. G. Zhang, Y. Chen, J. N. Su, W. W. Liu, T. H. Zhang, F. Qi, and Y. G. Wang, Interfacial stress transfer in a graphene nanosheet toughened hydroxyapatite composite, Applied Physics. Letters. 105, 161908 (2014). https://doi.org/10.1063/1.4900424

[27] X. Huang, X. Qi, F. Boey and H. Zhang, Graphene based composites, Chemical. Society Reviews. 41 (2012) 666–686. https://doi.org/10.1039/C1CS15078B

[28] Y. Wang, Z. H. Li, J.Wang, J. H. Li, Y. H. Lin, Graphene and graphene oxide: biofunctionalization and applications in biotechnology, Trends in Biotechnology. 29 (2011) 205–212 https://doi.org/10.1016/j.tibtech.2011.01.008

[29] H.S. Dong, S.J.Qi, Realising the potential of graphene-based materials for bio surfaces – A future perspective, Bio surface and Biotribology 1 (2015) 229–248. https://doi.org/10.1016/j.bsbt.2015.10.004

[30] K. Pavankumar, K. Venkateswarlu, N. Rameshbabu and V. Muthupandi, X-ray Peak Broadening and in-vitro Dissolution Studies of Thermally Stabilized Nanocrystalline Carbonated Hydroxyapatite, Key Engineering Materials, 493-494 (2012) 739-745. http://www.scientific.net/KEM.493-494.739

[31] H.Sirajunisha, P.Sakthivel and T.Balakrishnan, structural, photoluminescence, antibacterial and biocompatibility properties of HAp-Zn-rGO Nanocomposites, Journal ofMaterialsScience:Materials in Electronics 32(4),(2021) 5050-64 http:/doi.org/10.1007/s10854-021-05239-4

[32] Y. Weilin, S. TuanWei, Q. Chao, D. Zhenyu, Z. Huakun, Z. Shichang, S. Zhongmin, Z. Ying-Jie, Evaluation of zinc- doped mesoporous hydroxyapatite microspheres for the con- struction of a novel biomimetic scaffold optimized for bone augmentation. InternationalJournal of Nanomedicine. 12, 2293–2306 (2017). https://doi.org/10.2147/IJN.S126505

[33] Lu YP, Li MS, Li ST, Wang ZG, **Zhu RF,** Plasma-sprayed hydroxyapatite+titania composite bond coat for hydroxyapatite coatingon titanium substrate**,** Biomaterials. 25 (2004) 393-403. doi: 10.1016/j.biomaterials.2003.10.092.

[34] Leila Melo da Silva, Débora dos Santos Tavares, Euler Araujo dos Santos, "Isolating the Effects of Mg_{2+}, Mn_{2+} and Sr_{2+} Ions on Osteoblast Behavior from those Caused by Hydroxyapatite Transformation", Materials Research, 23 (2020) 1-10. https://doi.org/10.1590/1980-5373-MR-2020-0083

[35] V.D. Mote, Y.Purushotham, B.N. Dole, Williamson-Hall analysisinestimationoflatticestraininnanometersizedZnO particlesJournal ofTheorical. Applied Physics. 6, 1–8 (2012). https://doi.org/ 10.1186/2251-7235

[36] July Andrea Rincón-López, Jennifer Andrea Hermann-Muñoz, Astrid Lorena Giraldo-Betancur, Andrea De Vizcaya-Ruiz , Juan Manuel Alvarado-Orozco and Juan Muñoz-Saldaña, Synthesis, Characterization and In Vitro Study of Synthetic and Bovine-Derived Hydroxyapatite Ceramics: A Comparison, Materials. 11(2018) 333-350. doi:10.3390/ma11020333

[37] K. KaviRasu, P. Sakthivel, G.K.D.P. Venkatesan, Effect of Pd^{2+} co-doping on the structural and optical properties of Mn2+:ZnS nanoparticles, Optics & Laser Technology. 130 (2020) 106365. https://doi.org/10.1016/j.optlastec.2020.106365

[38] Mohammed Tareque Chowdhury , Md. Abdullah Zubair , Hiroaki Takeda, Kazi Md. Amjad Hussain, and Md. Fakhrul Islam, "Optical and structural characterization of ZnSe thin film fabricated by thermal vapour deposition technique", AIMS Materials Science, , 4(5) (2017) 1095-1121.DOI: 10.3934/matersci.2017.5.1095

[39] G.K. Williamson and W.H. Hall, X-ray line broadening from aluminium and wolfram, ActaMetallurgica. 1 (1953) 22–31. https://doi.org/10.1016/ 0001-6160(53) 90006-6

[40] P. Sakthivel, K. KaviRasu, G.K.D. P. Venkatesan, A. Viloria, Influence of Ag^{+} and Mn^{2+} ions on structural, optical and photoluminescence features of ZnS quantum dots, SpectrochimicaActa A, 241 (2020) 118666. https://doi.org/10.1016/j.saa.2020.118666.

[41] Anmin Hu, Ming Li, Chengkang Chang, Dali Mao, Preparation and Characterization of a Titanium-Substituted Hydroxyapatite Photocatalyst, Molecular Catalysis,267(2007) 79-85. DOI: 10.1016/j.molcata.2006.11.038

[42] E.S. Thian, T.Konishi, Y.Kawanobe, Zinc-substituted hydroxyapatite: a biomaterial with enhanced bioactivity and antibacterial properties.Journal of Materials Science.-Materials in Medicine 24, 437–445 (2013).https://doi.org/10.1007/s10856-012-4817-x

[43] H.-Y. Ye, Y. Zhang, D.-W. Fu and R.-G. Xiong, Angew.Hybrid Inorganic−Organic Materials with an Optoelectronically Active Aromatic Cation: $(C_7H_7)_2SnI_6$ and $C_7H_7PbI_3$ Chemie International Edition., **53** (2014) 11242–11247 https://doi.org/10.1021/ic5025795

[44] I. Devadoss, P. Sakthivel, S.P. Sheeba, Influence of Sn^{2+} ion on structural, morphological and optical characteristics of $Cd0.9{-}xZn0.1SnxS$ $(0 \le x \le 0.06)$ quantum dots. Indian Journal of Physics (2020). https://doi.org/10.1007/s12648-020-01735-1

[45] S. T. Hojati, H. Alaghemand, F. Hamze, F. A. Babaki, R. Rajab-Nia, M.B. Rezvani, M. Kaviani, M. Atai, Physical and mechanical properties of flowable resin composites containing zinc oxide nanoparticles, Dental Materials. 29 (2013) 495–505. https://dx.doi.org/10.1016/j.dental.2013.03.011

[46] A. K. Chaubey, P. Konda Gokuldoss, Z. Wang, S. Scudino, N. K. Mukhopadhyay, J.Eckert,*Effect of Particle Size on Microstructure and Mechanical Properties of Al-Based Composite* Reinforced with 10 Vol. % Mechanically Alloyed Mg-7.4% Al Particles, *Technologies.* 4 (2016) 37. https://doi.org/10.3390/technologies.4040037

[47] *M. E. Zilm, L. Chen, V. Sharma, A. McDannald, M. Jain, R. Ramprasada and M. Wei, Hydroxyapatite substituted by transition metals: experiment and theory, Physical Chemistry Chemical Physics. 18 (2016) 16457-16465. https://doi.org/10.1039/C6CP00474A*

[48] *B. Fu, Xuemei Sun, W. Qian, M. Hannig, Evidence of chemical bonding to hydroxyapatite by phosphoric acid esters, Biomaterials 26 (2005) 5104-10. https://doi.org/10.1016/j.biomaterials.2005.01.035*

[49] *T. J. Webster, E. A. Massa-Schlueter, J. L. Smith, and E. B. Slamovich, Osteoblast response to hydroxyapatite doped with divalent and trivalent cations, Biomaterials 25, (2004) 2111–2121.* https://doi.org/10.1016/j.biomaterials.2003.09.001

[50] S. Dasgupta, S. S. Banerjee, A. Bandyopadhyay, and S. Bose, Zn- and Mg-doped hydroxyapatite nanoparticles for controlled release of protein, Langmuir 26 (2010) 4958– 4964. https://doi.org/10.1021/la903617e

[51] E. Stoyanov, F. Langenhorst, G. Steinle-Neumann; The effect of valence state and site geometry on Ti $L_{3,2}$ and O *K* electron energy-loss spectra of Ti_xO_y phases. American Mineralogist . 92 (2007) 577–586. doi: https://doi.org/10.2138/am.2007.2344

[52] V. Cantavella, J. Carda, G. Monrós, M. A. Tena, P. Escribano and J. Alarcón , Zr^{4+} and Ti^{4+} substitution in gallium garnets,Journal of Materials Chemistry.3 (1993) 1059-1064. https://doi.org/10.1039/JM9930301059

[53] M.V. Chaikinaa, N.V. Bulinaa, IYu. Prosanova, O.B. Vino-kurovaa, A.V. Ishchenko, Structure formation of zinc-substituted hydroxyapatite during mechanochemicalsynthesis.Inorganic. Materials. 56, 402–408 (2020). https://doi.org/10.1134/S0020168520040044

[54] J. Terra, G. B. Gonzalez, A. M. Rossi, J. G. Eon and D. E. Ellis, Theoretical and experimental studies of substitution of cadmium hydroxyapatite,*Physical Chemistry Chemical Physics.* **12** (2010) 15490–15500.

[55] M. Matos, J. Terra, D.E. Ellis, Mechanism of Znstabilization in hydroxyapatite and hydrated (0 0 1) surfaces of hydrox- yapatite. Journal of. Physics: Condensed Matter. 22, 145502 (2010). https://doi.org/10.1088/0953-8984/22/14/145502

[56] Z. Sui, Wu. Jizhou, X. Wang, R. Dai, Z. Wang, X. Zheng, Z. Zhang, Cyclic phase transition from hexagonal to orthorhombic then back to hexagonal of EuF3 while loading uniaxial pressure and under high temperature. Journal ofPhysical.ChemistryC.120,18780–18787(2016).https://doi.org/10.1021/acs.jpcc.6b05907

[57] K. MinNam, W. SeokSeo, H. Song, J.T. Park, Non-native transition metal monoxide nanostructures: unique physico- chemical properties and phase transformations of CoO, MnOandZnO.NPGAsiaMaterials.9,e364(2017).https://doi.org/10. 1038/am.2017.38

[58] Z. Radovanovic, D. Veljovic, B. Jokic, S. Dimitrijevic, G. Bogdanovic, V. Kojic, R. Petrovic, D. Janackovic, Biocom- patibility and antimicrobial activity of zinc (II)-doped hydroxyapatite, synthesized by a hydrothermal method. Journal oftheSerbian Chemical Society. 77, 1787–1798 (2012). https://doi.org/10.2298/JSC121019131R

[59] Leila Melo da Silva, Débora dos Santos Tavares, Euler Araujo dos Santos, Isolating the Effects of Mg^{2+}, Mn^{2+} and Sr^{2+} Ions on Osteoblast Behavior from those Caused by Hydroxyapatite Transformation, .MaterialsResearch. 23(2) 1-10 (2020) : e20200083 DOI: https://doi.org/10.1590/1980-5373-MR-2020-0083

[60] Shuxia Yin, Donald E. Ellis, First-principles investigations of Ti-substituted hydroxyapatite electronic structure,*Physical Chemistry Chemical Physics.*, 12 (2010) 156–163. https://doi.org/10.1039/B915171K

[61] Mingzheng Ge, Chunyan Cao, Jianying Huang, Shuhui Li, Zhong Chen, KeQin Zhang, Al-Deya and Yuekun Lai, A Review of One-dimensional TiO_2 Nanostructured Materials for Environmental and Energy Applications, Journal of Materials Chemistry A, 00 (2013) 1-27. https://doi.org/10.1039/x0xx00000x

[62] C. Rey, V. Renugopalakrishnan, B. Collins, and M. Glimcher, Fourier transform infrared spectroscopic study of the carbonate ions in bone mineral during aging, Calcified Tissue International. 49 (1991) 251–258. https://doi.org/10.1007/BF02556214

[63] J. C. Merry, I. R. Gibson, S. M. Best, and W. Bonfield, Synthesis and characterization of carbonate hydroxyapatite, Journal of Materials Science: Materials in. Medicine. 9, 779–783 (1998). https://doi.org/10.1023/A:1008975507498

[64] R. David,G. Yong, M. Michelle,G. Graeme, Z. Zhijuan, M. Daniel, G. Eric, L. Jing, G. Martha, D. Gerard, Photochemical Water Oxidation by Crystalline Polymorphs of Manganese Oxides: Structural Requirements for Catalysis. Journal of American Chemical Society.135 (2013) 3494-3500. https://doi.org/10.1021/ja310286h

[65] N. Rameshbabu, T.S.Sambath Kumar, K.Prasad Rao, Synthesis of nanocrystalline Fluorinated hydroxyapatite by microwave processing and its in vitro dissolution study, Bullatin of Materials Science. 29 (2006) 611–615. https://www.ias.ac.in/ article/ full text/boms/029/06/0615.

[66] H. Eslami, M. Solati-Hashjin, M. Tahriri, Synthesis and characterization of fluorinated Hydroxyapatite powder by a modified wet-chemical process, Journal of Ceramic. Processing. Research, 9 (2008) 224–229. http://www.ijps.ir/article_2023_96d33098f13732ad0da4f43ff361d44b

[67] S. Shahid, S.A. Khan, W. Ahmad, U. Fatima, S. Knawal, Size-dependent bacterial growth inhibition and antibacterial activity of Ag-doped ZnO nanoparticles under different atmospheric conditions. Indian Journal of Pharmaceutical Science. 80, 173–180 (2008).

https://doi.org/10.4172/pharmaceutical-sciences.1000342

[68] CelaletdinErgun,Effect of Ti ion substitution on the structure of hydroxylapatite, Journal of the Europian Ceramic Society. 28 (2008) 2137–2149. https://doi.org/10.1016/j.jeurceramsoc.2008.03.007

[69] R.Mann, D.Mitsdis, Z.Xie, O.McNeily, Y. Hau Ng, R.Amal,C.Gunavan, "Antibacterial Activity of Reduced Graphene Oxide", Journal of Nanomaterials. 2021,(2021) http://doi.org/10.1155/2021/9941577

[70] J. H. Lee, Y-C. Shin, O. S. Jin, S. H. Kang, Yu-S. Hwang, J-C. Park, S. W. Hong, D-W. Han, Reduced graphene oxide coated hydroxyapatite composites stimulate spontaneous osteogenic differentiation of human mesenchymal stem cells, Nanoscale. 7(2015) 1–9. https://doi.org/10.1039/C5NR01580D

[71] A. Hu, M. Li, C. Chang, and D. Mao, "Preparation and characterization of a titanium-substituted hydroxyapatite photocatalyst," Journal of Molecular Catalysis A: Chemical. 267 (2007) 79–85. https://doi.org/10.1016/j.molcata.2006.11.038

[72] G.Qing, X. Zhao, N.Gong, J.Chen, X. Li, Y.Gan, Y.Wang, Z.Zhang, Y.Zhang, W.Guo, Thermo-responsive triple-function nanotransporter for efficient chemo-photothermal therapy of multidrug-resistant bacterial infection. Nature Communications. 10 (2019) 4336. https://doi.org/10.1038/s41467-019-12313-3

[73] D. W. Boukhvalov, D. M. Korotin, A. V. Efremov, E. Z. Kurmaev, Ch. Borchers, I. S. Zhidkov, D. V. Gunderov, R. Z. Valiev, N. V. Gavrilov, and S. O. Cholakh, Modification of titanium and titanium dioxide surfaces by ion implantation: Combined XPS and DFT study, Physica Status Solidi (B). (2014) 1–7. https://doi.org/10.1002/pssb.201451362

[74] D. Arcos, M. Vallet-Reg´ı, Substituted hydroxyapatite coatings of bone implants. Journal of Materials Chemistry. B 8, 1–45 (2020). https://doi.org/10.1039/C9TB02710F

[75] J.H. Lee, Y.C. Shin, S.-M. Lee, O.S. Jin, S.H. Kang, S.W. Hong, C.-M. Jeong, J.B. Huh, D.W. Han, Enhanced osteo- genesis by reduced graphene oxide/hydroxyapatite nanocomposites. Scientific Reports. 5, 8833 (2015). https://doi.org/10.1038/srep18833

***